Effect of $C13^2$-Stereochemistry on the Molecular Properties of Chlorophylls

Hiroyasu Furukawa,[#] Toru Oba,*[,†,##] Hitoshi Tamiaki,[†] and Tadashi Watanabe*

Institute of Industrial Science, The University of Tokyo, Tokyo 106-8558

†Department of Bioscience and Biotechnology, Faculty of Science and Engineering, Ritsumeikan University, Kusatsu, Shiga 525-8577

(Received December 27, 1999)

To elucidate the origin of differences in the monomeric properties of chlorophyll *a* and *a'* (Chl *a*/*a'*; $C13^2$-(*R*/*S*)-epimers of Chl *a*), a series of Zn–Chl derivatives possessing a variety of $C13^4$ substituents were prepared. The (*S*)-epimers gave absorption and emission bands at slightly longer wavelengths than the corresponding (*R*)-epimers. The (*S*)-epimers had more intense CD peaks than the (*R*)-epimers. In comparison with Zn–Chl *a*/*a'* ($C13^4$–Me), Zn–Chl with a bulky 2,4-dimethyl-3-pentyl moiety at the $C13^4$-position showed a greater difference between the ^{13}C NMR chemical shifts of the epimers. These spectral differences between the (*R*)- and (*S*)-epimers were attributed to ruffling of the chlorin macrocycle, arising from a steric repulsion between the $C13^2$ and C17 moieties. The trend of the rate constant of epimerization, isomerization at the $C13^2$ position, in the $C13^4$-substituted Zn–Chls is in line with the above interpretation. The relationship between the spectroscopic and kinetic results and the distortion of the macrocycle is schematically represented.

The stereochemistry of chlorophylls (Chls) and bacteriochlorophylls (BChls) is an important aspect in the research of their photosynthetic functions. To date the $C3^1$- and $C13^2$-epimers of Chl derivatives have been found in vivo (Fig. 1). The $C3^1$-stereochemistry of chlorosomal Chls may closely correlate to the antenna function through the self-assembly of the Chls with the intermolecular linkages involving the $C3^1$-moiety.[1—3] The $C13^2$-(*S*)-epimers of Chl *a* and BChl *g*, named Chl *a'* and BChl *g'*, respectively, were found in the core parts of the reaction center complexes of photosystem I and heriobacteria,[4—7] and the in vivo functions of the minor epimers have attracted much attention in recent years.

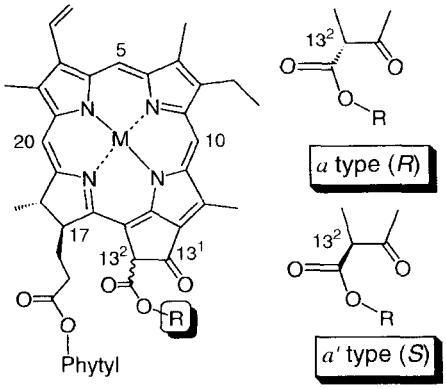

Fig. 1. Molecular structure of Zn–Chl *a* and *a'* with partial numbering according to the IUPAC system. Chl *a*/*a'*, M = Mg, R = Me; synthesized Zn–Chl *a*/*a'* derivatives, M = Zn, R = Me, Et, *i*Bu, *neo*Pn, $C_{10}H_{21}$, *i*Pr, 2,4-dimethyl-3-pentyl, 2,2,2-trichloroethyl, benzyl.

Present address: Department of Applied Chemistry, Faculty of Science and Engineering, Waseda University, Tokyo 169-8555.
Present address: Department of Applied Chemistry, Faculty of Engineering, Utsunomiya University, Utsunomiya, Tochigi 321-8585, Japan.

Chl *a'* is thermodynamically less stable than Chl *a* (the equilibrium Chl *a'* mole fraction = 0.24 in diethyl ether, see Ref. 8), since the $C13^2$-methoxycarbonyl moiety and the C17-propionate with a long phytyl chain in Chl *a'* both protrude to the same side of the chlorin (17,18-dihydroporphyrin) macrocycle. The epimers can be distinguished from each other by NMR[9—11] and circular dichroism (CD)[11,12] spectra, the rate of pheophytinization (demetallation),[13—15] and the elution behaviors in high-performance liquid chromatography (HPLC).[4,12,16] Chl *a* and *a'* also showed clear differences in their self-assemblies in aqueous alcohols.[17—21] Monomeric Chl *a'* gives only slightly different visible absorption and fluorescence spectra in comparison with Chl *a*. Though it is reasonable to attribute some of these differences, such as the HPLC elution order and the aggregation behavior, to the steric effects of the $C13^2$ stereochemistry, little is known about the origin of the differences observed in NMR and absorption spectra. Hanson reported that ruffling of the macrocycle of (B)Chl changes absorption spectra through changes in the MO levels,[22] as was supported by analyses of seven BChl molecules in FMO protein.[23] Tamiaki et al. reported that steric repulsion between the C3/C18-methyl groups and the C20-moiety of synthetic Zn–C20-halogenochlorins (C20: F, Cl, Br) distorted the macrocycle, resulting in changes in the absorption spectra.[24,25] Hynninen

suggested that steric repulsion between the C13²- and C17-moieties induces ruffling of the chlorin macrocycle.[10,26] In this context, the size of the C13²-moiety may have a crucial role in determining the electronic properties of Chls which are in close relationship with their in vivo functions.

In this work, we synthesized Chl *a*/*a'* derivatives possessing a series of C13⁴-substituents. The properties of these compounds were characterized by visible absorption, florescence emission, CD and ^{13}C NMR spectroscopies, as well as epimerization behaviors. The results confirmed that the steric hindrance between the C17-phytyl chain and C13² moiety induces ruffling of the chlorin macrocycle which in turn affects the electronic properties of Chls.

Results

Syntheses of Zn-Chlorins. The C13²-methoxycarbonyl group (M = H_2, R = Me, Fig. 1) of Pheo *a* (C17-phytyl ester compound **1**) was converted to other alkyl esters; ethyl (**2**, R = Et), isobutyl (**3**, R = *i*Bu), neopentyl (**4**, R = *neo*Pn), decyl (**5**, R = C_{10}), isopropyl (**6**, R = *i*Pr), 2,4-dimethyl-3-pentyl (**7**, R = CH*i*Pr_2), 2,2,2-trichloroethyl (**8**, R = CH_2CCl_3), and benzyl (**9**, R = Bzl) (Table 1). Pheo *a* was transesterified in toluene in the presence of 2-chloro-1-methylpyridinium iodide, and 4-(dimethylamino)pyridine, as reported for the C13²-substitution of methyl pheophorbide *a* (C17-methyl ester compound).[27,28] The C13⁴-methyl proton resonance peak of Pheo *a* (3.90 ppm) disappeared during the course of the reaction, and the NMR peaks of new C13⁴-moieties appeared: e.g., 4.79 ppm (CH-13⁴ for **7** (R = CH*i*Pr_2)). FAB-mass spectrometry clearly confirmed the formation of the desired compounds: e.g., 954.3 for **7** (R = CH*i*Pr_2). The C13²-transesterification was successfully performed despite the presence of the long phytyl chain ($C_{20}H_{39}$). The yields of the transesterification ranged from 21 to 66%, depending on the alcohol condensed. 2,4-Dimethyl-3-pentyl (**7**) and benzyl alcohols (**9**) reacted with a relatively high yield, while ethyl (**2**), isobutyl (**3**), and 2,2,2-trichloroethyl alcohols (**8**) did so less efficiently. This trend is in accordance with that reported by Shinoda et al.[27] The yields for the reaction of Pheo *a* were lower than the corresponding transesterification in methyl pheophorbide *a*; this may be attributed to the steric hindrance between the C13²-moiety and C17-long alkyl chain of Pheo *a*.

The thus-obtained Pheo *a* derivatives were metallated with zinc acetate in methanol.[25,29] The reasons for choosing of Zn-complexes were four-fold: Zn–Chl is superior to the Mg-complexes in (1) the ease of preparation and (2) molecular stability; (3) the Zn atom in Zn–Chl can usually take only one axial ligand to form a five-coordinated state; (4) Zn–Chl has similar spectroscopic properties to Mg–Chl. The C13²-(*R*)- and (*S*)-epimers of the Zn–Chls were separated by normal-phase HPLC (hexane/acetone/methanol = 100 : 5 : 1.5 or 100 : 2 : 0.8). Synthetic Zn–Chls **2**—**9** were eluted earlier than **1** (R = Me), and all of the (*S*)-epimers were eluted more rapidly than the corresponding (*R*)-epimers. The syntheses of these Zn-complexes were also confirmed by ^{1}H NMR and FAB-mass spectroscopies.

Table 1. Transesterification of Pheo *a*

Entry	Symbol	ROH	Yeild/%
1	Me	—	—
2	Et	C_2H_5OH	22
3	*i*Bu	$(CH_3)_2CHCH_2OH$	21
4	*neo*Pn	$(CH_3)_3CCH_2OH$	43
5	C_{10}	$C_{10}H_{21}OH$	40
6	*i*Pr	$(CH_3)_2CHOH$	46
7	CH*i*Pr_2	$((CH_3)_2CH)_2CHOH$	66
8	CH_2CCl_3	CCl_3CH_2OH	26
9	Bzl	$C_6H_5CH_2OH$	55
10	Pyro	—	95

Visible Absorption and Fluorescence Spectra of Zn–Chlorins in Methanol. Figure 2 illustrates the visible absorption and fluorescence spectra of natural-type **1*R*** (Zn–Chl *a*; R = Me, C13²-(*R*)-epimer). The Q_y and Soret absorption peaks of **1*R*** in methanol located at 658.2 and 427.5 nm (solid curve) blue-shifted from those of Chl *a* (**11*R***, M = Mg, 665.7 and 432.3 nm). The molar extinction coefficient of the 658-nm band was 7.15×10^4 M^{-1} cm^{-1} (1 M = 1 mol dm^{-3}). Because the C13²-moiety is out of the π-electronic system, the absorption spectral shapes of **1*R*** and **1*S*** (Zn–Chl *a'*; C13²-(*S*)-epimer) were almost identical to each other. One should note that the Q_y peak of **1*S*** is located at a longer wavelength by 0.4 nm ($\Delta\lambda$; 9 cm^{-1}) than that of **1*R*** (Table 2). The difference between the Soret peak positions of the *R*/*S* epimers was more modest than that of the Q_y peak. Such slight differences are reminiscent of similar ones between Chl *a* and *a'* found by Hynninen et al. (**11*R***, 664.1 nm; **11*S***, 664.7 nm in tetrahydrofuran (THF)).[11] The fluorescence emission spectra (broken curve in Fig. 2) revealed similar deviations between the band positions of **1*R*** and **1*S***. The Q_y (0–0) emission band of **1*R*** was at 665.3 nm, 9-nm shorter wavelength than **11*R***, while that of **1*S*** was at 666.2 nm ($\Delta\lambda$ = 0.9 nm, 20 cm^{-1}). The Q_y fluorescence intensities of **1*R*** and **1*S*** were nearly the same (Φ = 0.22).

The C13⁴-substitution changed the value of $\Delta\lambda$. Figure 3a represents the visible absorption spectra of **7*R*/*S*** (R = CH*i*Pr_2) in methanol. Replacement of the C13⁴–Me

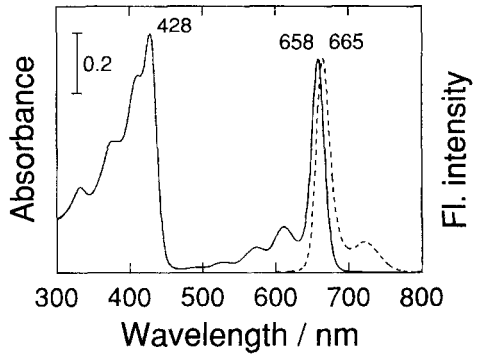

Fig. 2. Visible absorption and fluorescence spectra of **1*R***. Solid curve, absorption (10 μM); broken curve, fluorescence emission (0.74 μM, excited at 425 nm), recorded in methanol at room temperature.

Table 2. Comparison of the Visible Absorption, Fluorescence Emission, and CD Spectra of a Series of Zn–Chls in Methanol

Entry	Symbol	Absorption				Emission				CD (Soret)		CD (Q_y)	
		(*R*)	(*S*)	$\Delta\lambda$		(*R*)	(*S*)	$\Delta\lambda$		(*R*)	(*S*)	(*R*)	(*S*)
		nm	nm	nm	cm^{-1}	nm	nm	nm	cm^{-1}	mdeg	mdeg	mdeg	mdeg
1	Me	658.2	658.6	0.4	9	665.3	666.2	0.9	20	3.2	7.0	−1.5	−6.6
2	Et	658.1	659.0	0.9	21	665.5	666.6	1.1	25	3.1	8.1	−1.2	−8.0
3	*i*Bu	658.1	658.9	0.8	18	665.5	666.6	1.1	25	2.9	8.1	−0.8	−8.2
4	*neo*Pn	658.1	659.0	0.9	21	665.3	666.5	1.2	27	2.9	8.2	−0.7	−8.6
5	C_{10}	658.1	659.0	0.9	21	665.5	666.6	1.1	25	2.8	8.5	−0.6	−9.0
6	*i*Pr	658.2	659.3	1.1	25	665.4	666.7	1.3	29	3.2	8.6	−0.8	−8.7
7	$CHiPr_2$	657.9	659.5	1.6	37	665.1	667.0	1.9	43	3.1	10.0	−0.2	−9.8
8	CH_2CCl_3	658.4	659.0	0.6	14	665.8	666.3	0.5	11	2.8	8.0	−0.7	−8.3
9	Bzl	658.6	659.2	0.6	14	666.1	666.7	0.6	14	2.7	7.9	−0.1	−8.7
10	Pyro	658.6	—	—	—	666.0	—	—	—	3.7	—	−4.4	—

with $CHiPr_2$ shifted the Q_y absorption peak positions of the (*S*)-epimer (658.6 → 659.5 nm) and, more modestly, of the (*R*)-epimer (658.2 → 657.9 nm). The Q_y peak positions of **7*R*** differed from that of **7*S*** by 1.6 nm. Each $C13^4$-substituted Zn–Chl showed such a deviation ($\Delta\lambda$) between the (*R*)- and (*S*)-epimers (Table 2). Roughly, the larger was the size of the $C13^4$-substituent, the larger did the $\Delta\lambda$ become: the deviation increased in going from **1** (R = Me, $\Delta\lambda$ = 9 cm^{-1}) to **2**—**5** (with primary alkyl groups at the $C13^4$-position; ca. 20 cm^{-1}), and to **6** and **7**, (with secondary alkyl groups; 25 and 37 cm^{-1}, respectively). For **8** and **9**, having electron withdrawing and aromatic groups at $C13^4$, the Q_y peak positions of (*R*)- and (*S*)-epimers differ by 14 cm^{-1}.

Similar deviations were observed in the fluorescence emission spectra (Fig. 3 and Table 2). The deviations ($\Delta\lambda$) of each epimer pair in the fluorescence spectra, larger than those in the absorption spectra, became greater with an increase in the size of the $C13^4$ substituent (20 cm^{-1} for **1** to 43 cm^{-1} for **7**). The Q_y emission peak positions of the (*R*)-epimers were nearly unchanged by any $C13^4$-substituents. Little change was detected for the Stokes shifts (ca. 170 cm^{-1}) and the quantum yields through $C13^4$-substitutions.

$C13^2$-Demethoxycarbonyl derivative **10** (Zn–pyroChl *a*) was also examined as a reference. Removal of the $C13^2$-methoxycarbonyl group gave the Q_y absorption and emission bands almost in between the peak positions of the (*R*)- and (*S*)-epimers.

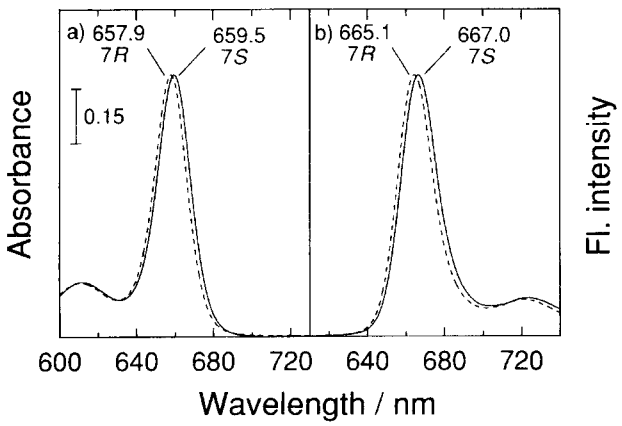

Fig. 3. Visible absorption and fluorescence emission spectra of **7** (R = $CHiPr_2$). a) absorption (10 μM): broken curve, **7*R***; solid curve, **7*S***; b) fluorescence emission (0.74 μM, excited at 425 nm): broken curve, **7*R***; solid curve, **7*S***. The spectra were recorded in methanol at room temperature.

Solvent Effect. Such spectral differences in the Q_y peak positions between the (*R*)- and (*S*)-epimers were observed irrespective of the solvent (Table 3). Compound **1*R*** gave the Q_y absorption peaks at 656.4 and 658.1 nm in THF and benzene, respectively, and the $\Delta\lambda$'s of **1** were 23 cm^{-1} (THF) and 25 cm^{-1} (benzene). The values in THF and benzene also increased with increasing the size of the $C13^4$-substituent, and reached a maximum in the case of **7** (R = $CHiPr_2$, $\Delta\lambda$ = 51 cm^{-1}). Essentially the same behaviors were observed in the fluorescence spectra: in going from **1** to **7**, 21 → 52 cm^{-1} (THF) and 25 → 50 cm^{-1} (benzene). The stokes shifts and the quantum yields were nearly independent of the $C13^4$-substituents in both solvents.

A reference compound **10** in THF and benzene gave the Q_y absorption and emission bands at wavelengths shorter than those of **1*R*** (R = Me), as in a comparison of Mg–pyroChl *a* with **11*R*** in diethylether:[30] e.g., the Q_y absorption (emission) peak of **10** in benzene, 656.8 (662.8) nm.

CD Spectra of Zn-Chlorins. Figures 4a, 4b, 4c, and 4d show the CD spectra of the $C13^4$-substituted Zn–Chls in methanol. Both epimers **1*R*** and **1*S*** (R = Me) exhibit CD spectra with characteristics essentially the same as those of **11*R*** and **11*S***, respectively (Fig. 4a).[11,12,31] Both **1*R*** and **1*S*** gave the Q_y trough at 660 nm, and the intensity of the former was much weaker than the latter (Table 2). The (*S*)-epimer **1*S*** gave a set of positive and negative spectral components in the Soret region (431 and 382 nm), while **1*R*** showed less intense, positive signals (peaking at 423 nm) and no negative peak. The (*S*)-epimer **1*S*** also gave a relatively smaller, positive CD component at 572 nm (presumably assignable to the $Q_x(0\text{–}0)$ band), where **1*R*** had no CD intensity. All CD components of **1*R*** (**1*S***) in the visible region were as intense as those of **11*R*** (**11*S***) in methanol.[17]

Little influence was observed on the CD spectral shape with regard to the $C13^4$-substitution: Each CD spectrum of the $C13^2$-(*R*)-epimers ($C13^2$-(*S*)-epimers) in the Soret and Q_y regions was similar in shape to that of **1*R*** (**1*S***). The $C13^4$-substitution, however, changed the CD intensities while main-

Table 3. Solvent Effect of the Visible Absorption and Fluorescence Emission Spectra of Zn–Chls

Entry	Symbol	Solvent	Absorption				Emission			
			(*R*)	(*S*)	$\Delta\lambda$		(*R*)	(*S*)	$\Delta\lambda$	
			nm	nm	nm	cm^{-1}	nm	nm	nm	cm^{-1}
1	Me	MeOH	658.2	658.6	0.4	9	665.3	666.2	0.9	20
7	CH*i*Pr$_2$	MeOH	657.9	659.5	1.6	37	665.1	667.0	1.9	43
10	Pyro	MeOH	658.6	—	—	—	666.0	—	—	—
1	Me	Benzene	658.1	659.2	1.1	25	664.1	665.2	1.1	25
7	CH*i*Pr$_2$	Benzene	657.8	660.0	2.2	51	663.8	666.0	2.2	50
10	Pyro	Benzene	656.8	—	—	—	662.8	—	—	—
1	Me	THF	656.4	657.4	1.0	23	662.4	663.3	0.9	21
7	CH*i*Pr$_2$	THF	656.0	658.2	2.2	51	661.6	663.9	2.3	52
10	Pyro	THF	655.3	—	—	—	661.0	—	—	—

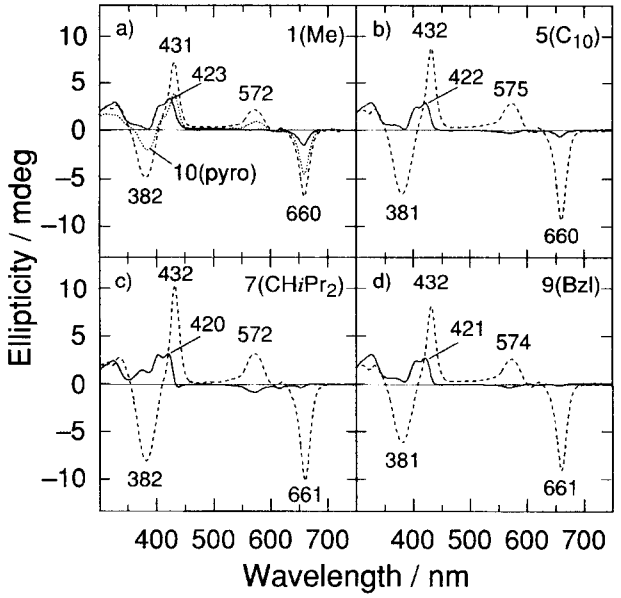

Fig. 4. Circular dichroism spectra of the Zn–chlorins. a) Solid curve, **1*R***; broken curve, **1*S***; dotted curve, **10**; b) solid curve, **5*R***; broken curve, **5*S***; c) solid curve; **7*R***; broken curve, **7*S***; d) solid curve, **9*R***; broken curve, **9*S***. The spectra were recorded in methanol at concentration of 10 μM at room temperature.

taining the spectral feature. As for the $C13^2$-(*R*)-epimers (solid curves in Figs. 4b, 4c, and 4d; Table 2), the intensities of the Q_y lobe of the $C13^4$-substituted chlorins (660—661 nm) were weaker than that of **1*R*** (R = Me). A negative CD band appeared at around 572—574 nm, and became stronger with increasing bulkiness of the $C13^4$-group. The Soret signals (at 420—423 nm) reduced their intensities much more modestly than those observed in the other regions. As for the $C13^2$-(*S*)-epimers (broken curves in Figs. 4b, 4c, and 4d; Table 2), the CD intensity of the Q_y trough increased in going from R = Me (**1*S***), to Et (**2*S***), C_{10} (**5*S***), and to CH*i*Pr$_2$ (**7*S***). The amplitudes of the CD bands in the Q_x (572—574 nm) and Soret region (431—432 nm and 381—382 nm) were also enhanced by the $C13^4$-substitution. Such tendencies were also observed for the THF and benzene solutions (data not shown).

It is noted that, in the Q_x and Q_y regions, the summation of the CD lobes of each epimeric pair of **1**—**9** approximately resembled to the CD signals of **10** (Zn–pyroChl *a*, dotted curve in Fig. 4a and Table 2).

Epimerization of Zn–Chlorins. Epimerization at the $C13^2$ position in the $C13^4$ substituted Zn–Chls was investigated by the use of triethylamine as a catalyst in diethyl ether. No pigment degradation other than epimerization occurred during the experiments.[12,16] The kinetics of epimerization was analyzed as in Ref. 32 on the basis of a pseudo-first-order reaction:

$$\text{Zn–Chl } a \underset{k'}{\overset{k}{\rightleftharpoons}} \text{Zn–Chl } a' \tag{1}$$

$$\ln\{([a]_t - [a]_\infty)/([a]_0 - [a]_\infty)\} = -(k+k')t, \tag{2}$$

$$[a]_\infty = k'/(k+k'). \tag{3}$$

Here, k and k' are the apparent pseudo-first-order rate constants. When $\ln\{([a]_t - [a]_\infty)/([a]_0 - [a]_\infty)\}$ is plotted as a function of time, the slope of a line gives the $-(k+k')$ value. Figure 5 depicts the rate constants $(k+k')$ of the nine Zn–Chls plotted against the concentration of triethylamine. The constants $(k+k')$ of all of these Zn–Chls increased linearly with an increase of the triethylamine concentration in the range of 0.01 to 0.2 mol dm^{-3}. The slopes of the lines were 1.00, demonstrating that epimerization proceeded via a general base catalysis:[13,32] Deprotonation at the $C13^2$-position by triethylamine yields an enol intermediate whose $C13^2$–$C13^3$ bond oriented coplanarly to ring V, and attack of proton to the sp^2-carbon at the $C13^2$ atom from either side of the macrocycle results in reproduction of the epimers.

Figure 5 also shows that the epimerization rate depended on the nature of the $C13^4$-moiety. The rate constants of epimerization of Zn–Chls with primary aliphatic groups at the $C13^4$-position (**2**—**5**) were close to that of Zn–Chl *a*/*a'* (**1**), while Zn–Chls of $C13^4$-secondary aliphatic groups isomerized more slowly (**6** and **7**; Table 4). Epimerizations of Zn–Chls possessing electron withdrawing and aromatic groups at the $C13^4$ position (**8** and **9**) were much more rapid than those of the other Zn–Chls: **8** (R = CH_2CCl_3) transformed roughly 9 times faster than **2** (R = Et).

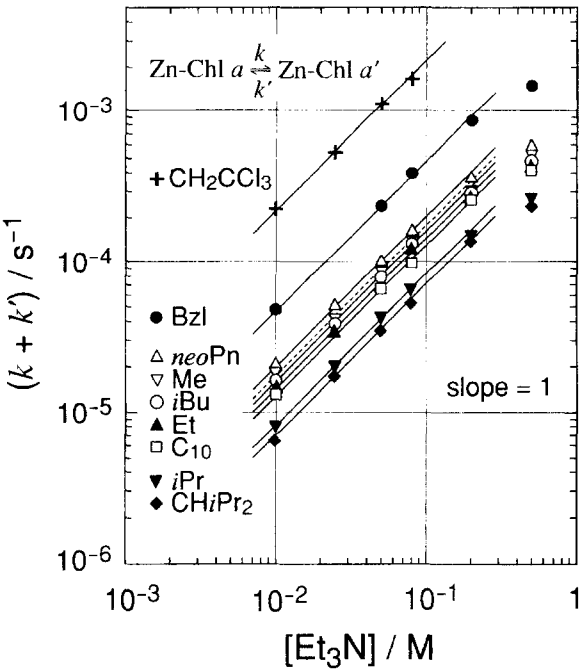

Fig. 5. Plots of the epimerization rate constants of a series of Zn–chlorins (**1**—**9**) against the concentration of triethylamine.

Table 4. Rate Constants, Equilibrium Composition, and Free Energy Difference for Epimerization of the $C13^4$-Substituted Zn–Chls

Entry	Symbol	$k+k'/s^{-1}$	$[a']_\infty$	ΔG°/kJ mol^{-1}
1	Me	1.4×10^{-4}	0.21	3.3
2	Et	1.3×10^{-4}	0.17	4.0
3	*i*Bu	1.4×10^{-4}	0.17	4.0
4	*neo*Pn	1.7×10^{-4}	0.16	4.1
5	C_{10}	9.8×10^{-5}	0.17	3.9
6	*i*Pr	6.7×10^{-5}	0.13	4.7
7	$CHiPr_2$	5.7×10^{-5}	0.03	8.6
8	CH_2CCl_3	1.1×10^{-3}	0.15	4.4
9	Bzl	4.0×10^{-4}	0.15	4.4

Structural Differences between a Pair of Epimers Detected by ^{13}C NMR Spectra. We measured the ^{13}C NMR spectra of **1** (Me) and **7** ($CHiPr_2$) in $CDCl_3/CD_3OD = 9:1$ (v/v) as representatives; the difference between the chemical shift of each resonance peak of $C13^2$-(*S*)- and (*R*)-epimers ($\Delta\delta$) is illustrated in Fig. 6. An open circle (a filled circle) is for a resonance peak of the carbon atom of an (*R*)-epimer situated at more downfield (upfield) than the corresponding NMR peak of the (*S*)-epimer, and the radius of the circle denotes the magnitude of the chemical shift difference.[33] Figure 6a illustrates the ^{13}C-chemical shift differences between **1*R*** and **1*S*** (R = Me). Most of the carbons at rings IV and V are marked by open circles, indicating that the resonance peaks of the skeletal carbons of the (*R*)-epimer were given at more downfield than the corresponding peaks of the (*S*)-epimer (e.g., $\Delta\delta$ = +0.6 ppm for the C17). The magnitudes of $\Delta\delta$ at rings IV and V were larger than those of rings I—III. These tendencies are similar to those observed for Chl *a*/*a'* (**11**, M = Mg, R = Me) in THF (e.g., $\Delta\delta$ = +0.7 ppm for the C17).[10]

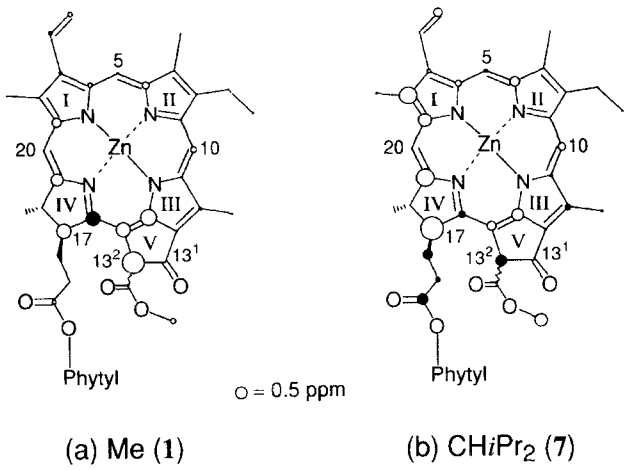

Fig. 6. Schematic representations of the ^{13}C chemical shift differences. a) **1*R/S*** (R = Me), b) **7*R/S*** (R = $CHiPr_2$).

Zn–Chl with the most bulky $C13^4$-substituent (2,4-dimethyl-3-pentyl group; **7*R/S***) showed another profile (Fig. 6b). The chemical shift differences at the C14, C15, and C16-positions reduced their magnitudes while maintaining the 'polarities' of $\Delta\delta$'s when comparing with those of **1*R/S***, whereas the C17 and C19 atoms enhanced the differences (e.g., **1**, $\Delta\delta$ = +0.7 ppm for the C14; **7**, +0.5 ppm for the C14; **1**, +0.5 ppm for the C19; **7**, +0.8 ppm for the C19). At the C17 and $C13^2$-positions, the 'polarities' of the differences between **7*R*** and **7*S*** were opposite to those of **1*R*** and **1*S***. The differences in the chemical shifts of the $C17^1$—$C17^3$ atoms of **7*R/S*** became more conspicuous compared with those of **1*R/S***. Relatively large $\Delta\delta$'s were detected at ring I ($\Delta\delta$ at the C1 and C2 positions: **7*R/S***, +0.6 and +0.8 ppm; **1*R/S***, +0.4 and 0.0 ppm).

A comparison of the results between **1*S*** and **7*S*** (**1*R*** and **7*R***) reveals that the structures of the (*S*)-epimers were more sensitive to $C13^4$-substitution than were the (*R*)-epimers: The chemical shift differences between the corresponding resonance peaks of **1*S*** and **7*S*** were larger than the differences between **1*R*** and **7*R*** ($\Delta\delta$ at the C2 position: **1*R/7R***, −0.1 ppm; **1*S/7S***, +0.6 ppm).

Discussion

Structural Differences between (*R*)- and (*S*)-Epimers of Zn–Chlorins. The chemical shift of a ^{13}C NMR peak depends on the electron density and the degree of the shielding of the carbon atom. It may be reasonable to assume that a set of molecules that can only be distinguished from the $C13^2$-stereochemistry causes only a small difference in the electron densities of the π-system atoms, as suggested by the fact that the magnitudes of the chemical shift differences between Chl *a*/*b* (C7-Me/CHO) were much larger than those between **11*R/S***,[9,34] **1*R/S***, or even between **7*R/S***. The deviations between the chemical shifts of the epimers observed in this study may dominantly be attributed to changes of the shielding effect arising from transformations of the 5- and 6-

membered rings of the chlorin macrocycle.[10]

Hynninen and Lötjönen had rationalized that the conformational changes in the macrocycle were induced by a steric repulsion between the C13²-moiety and C17-alkyl chain.[10] This view indicates that (1) the macrocycle of the (*S*)-epimer should be more distorted than that of the (*R*)-epimer, because the steric hindrance between the C13²-substituent and the nearby C17-phytyl chain is much greater in the C13²-(*S*)-epimer than in the C13²-(*R*)-epimer, and that (2) the ruffling should be much greater in compounds possessing a more bulky C13²-moiety; these points were indeed confirmed in the present work. The mechanism that causes the differences between the NMR peak positions of the (*R*)- and (*S*)-epimers is thus interpreted as follows. The repulsive force between the C13²- and C17-moieties makes these substituents escape from each other, to direct them to the periphery of the macrocycle, resulting in bending of the macrocycle. The influence of the repulsion may predominantly transform the reduced ring (ring IV) and ring V; this is supported by the crystal structure of ethyl chlorophyllide *a*[35] and by the molecular modeling calculations mentioned below.

We estimated the optimized molecular structures of the C13⁴ substituted Zn–Chls by molecular mechanics and molecular-orbital calculations (MM^+ and PM3, see Experimental section) to examine the difference between the macrocycle structures of the (*R*)- and (*S*)-epimers. The distance of each atom constituting a macrocycle (22 carbon atoms C1—C20, C13¹, and C13²) from a standard plane defined by nitrogen atoms N21—N24 was calculated. The averages of the distances were 4.0×10^{-2} Å for the (*R*)-epimers and 1.1×10^{-1} Å for the (*S*)-epimers, indicating that the (*S*)-epimers were much less planer than the (*R*)-epimers. It was found that rings IV and V were the most variable parts with changes at the C13²-moieties: the standard deviations at C13¹, C13, and C18 were 0.18, 0.14, and 0.13 Å, respectively, in contrast to the values at C3 (0.02 Å), C7 (0.05 Å), and C2 (0.05 Å), and the average dihedral angles between C13²C15–C16C17 were ca. −0.4 and ca. +3.8 degrees for the (*R*)- and (*S*)-epimers, respectively. C13²-Demethoxycarbonyl derivative **10** had the smallest average distance of 0.02 Å and a standard deviation of 0.01 Å, while the least-planer molecule was **7*S*** (average distance, 0.12 Å; standard deviation, 0.08 Å). We must be careful to interpret these simulations, because the calculations ignored the effects of solvent molecules, did not consider all possible conformations, and replaced the phytyl chain with a methyl group. However, these calculations seem to be consistent with the above interpretation for the NMR results.

Effects of the Macrocycle Ruffling on the Visible Absorption, Fluorescence, and CD Spectra. Hanson reported that a distortion of (bacterio)chlorin macrocycle raises the energy level of the highest occupied molecular orbital along with small change in the lowest unoccupied molecular orbital; such a change results in a red-shift of the Q_y band.[22] However, the (*R*)-epimers with C13⁴-aliphatic groups (**1**—**7**) gave the Q_y absorption and emission peaks approximately at the same wavelengths (absorption, 657.9—658.2 nm; emission, 665.1—665.5 nm in methanol), the Q_y peak positions of the (*S*)-epimers red-shifted with increasing bulkiness of the C13⁴-moiety, and reached maximum values for **6*S*** and **7*S*** that had secondary alkyl groups at the C13⁴-positions (Table 2). These findings can be attributed to the distortion of the macrocycles induced by the steric repulsion between the C13² and C17 moieties, as in case of Zn–20-halogenochlorins bearing steric interference between the C20 and C2/C18 moieties.[24,25] The deviations observed in the absorption and emission spectra of **8** and **9**, which have electron-withdrawing and aromatic substituents, originate from an electronic effect of the C13⁴-substituent.

The CD spectra of the C13⁴-substituted Zn–Chls can also be correlated to the ruffling of the macrocycle. The Soret CD signals of the (*S*)-epimers increased with an increase in the bulkiness of the C13² moiety (**1*S***—**9*S***), whereas those of the (*R*)-epimers changed only slightly in going from **1*R*** to **9*R*** (Table 2). Wolf et al. reported that the CD intensity in the Soret region strongly depended on the local structures at the C17- and C18-positions.[36] In this context, our findings suggest that the distortion at ring IV of the (*S*)-epimer became greater with strengthening of the steric repulsion between the C13²- and C17-moieties. This is in agreement with other results, including molecular modeling calculations.

The CD signal in the Q_y region also depended on the size of the C13⁴ moiety and the stereochemistry at the C13² position. The Q_y CD intensity of the (*S*)-epimer became more negative, while that of the (*R*)-epimer became less negative with an increase in the size of the C13⁴ moiety. Figure 7 shows difference CD spectra obtained by subtracting the spectrum of **10** from those of C13⁴-substituted Zn–Chls. The spectra of a pair of epimers looks like a mirror image. The (*R*)-epimers gave positive Q_y bands, while the (*S*)-epimers negative ones. The polarities of the Q_x and the Soret bands also depended on the chirality at the C13² position. These findings could be rationalized by invoking that the magnitudes and directions

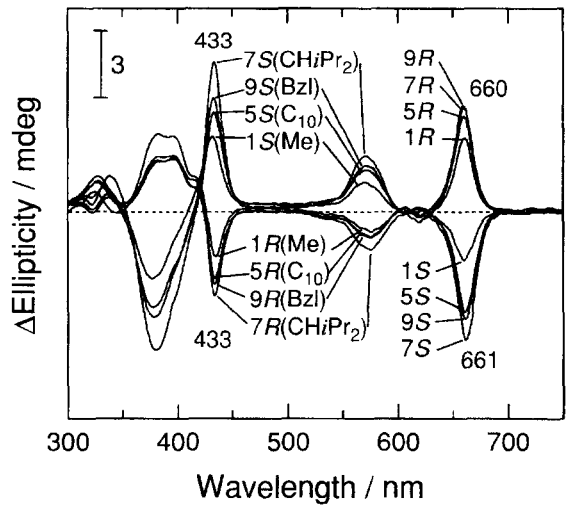

Fig. 7. Difference CD spectra of the C13⁴-substituted Zn–Chls, obtained by subtraction of the spectrum of **10** from each spectrum of **1** (R = Me), **5** (R = C_{10}), **7** (R = $CHiPr_2$), and **9** (R = Bzl).

of the electric and magnetic dipoles of the $C13^2$ moiety depended, in principle, on the size (and geometry) of the $C13^2$ substituent and on the chirality at the $C13^2$ position. The reference compound **10** may have an average structure of the (*R*)- and (*S*)-epimers, as supported by the above calculations. Any deviation from the complete mirror image may be due to a distortion of the macrocycle. These results will contribute to any theoretical examination of the CD spectra of Chls in the future studies.

Effects of Solvents. Methanol is a solvent that can make hydrogen-bondings with carbonyl groups of Chl as well as coordinate to the central metal atom of Chl, which differs from THF and benzene. It was observed that even in THF and benzene (*S*)-epimers gave the Q_y peak positions at wavelength longer than those of (*R*)-epimers and the deviation ($\Delta\lambda$) increased with an increase of bulkiness of the $C13^4$-substituent. These findings demonstrate that solvent effects are not primarily responsible for such spectral differences in the Q_y peak positions between (*R*)- and (*S*)-epimers.

The trend that the band positions of Zn–Chls (**1**—**9**) in THF were located at wavelength shorter than those in methanol and benzene is consistent with those reported for Mg–Chl.[37] Though it is unclear why the amplitude of the $\Delta\lambda$ value in methanol was smaller than those in THF and benzene (Table 3), the observation may be correlated to the possibilities that a distortion of the macrocycle alters (1) the intensity of the coordination interaction between a solvent molecule and the central Zn atom of the Chl, (2) the intensity of hydrogen bonding between a solvent molecule and the $C13^1$=O moiety of the Chl, and (3) the susceptibility of the Chls to the polarity of the solvent.

Epimerization Behaviors. An examination of the kinetics of epimerization of the $C13^4$-substituted Zn–Chl provides measures of stability of the compounds. Table 4 depicts the rate constants ($k+k'$) and the equilibrium composition $[a']_{eq}$ of a series of Zn–Chls. The value of $[a']_{eq}$ leads to the free-energy difference (ΔG°) of the epimeric pair:

$$\Delta G^\circ = -RT\ln K = -RT\ln\{[a']_{eq}/[a]_{eq}\}, \quad (4)$$

where R is the gas constant, T is temperature, and K is the equilibrium constant ($= [a']_{eq}/[a]_{eq}$). There is a rough tendency that the free energy difference increases with an increase in the size of the $C13^2$-moiety (Table 4). Zn–Chls **2**—**5** ($C13^2$-primary aliphatic esters) gave ΔG° of ca. 4 kJ mol^{-1}. Larger free energy differences were calculated for compounds **6** and **7**, the $C13^2$-secondary aliphatic esters (**7**: 8.6 kJ mol^{-1}). There is also a rough tendency that Zn–Chls possessing polar or aromatic groups at the $C13^4$-position epimerized more rapidly than those possessing apolar ones, and that Zn–Chls possessing $C13^4$-primary aliphatic groups did so more than those possessing $C13^4$-secondary aliphatic groups: compounds **8** and **9** gave much larger rate constants than those of **1**—**7** ($< 2\times10^{-4}$ s^{-1}) with keeping the free energy, and ($k+k'$) of compounds **1**—**4** (the $C13^4$-primary aliphatic derivatives, $> 1\times10^{-4}$ s^{-1}) were two-times larger than those of **6** and **7** (the $C13^4$-secondary aliphatic derivatives, ca. 0.6×10^{-4} s^{-1}).

The ΔG° value demonstrates the relative stabilities of a pair of epimers. The relative stabilities can be affected by ruffling of the macrocycle. The observed relationship between ΔG° and the size of the $C13^2$-moiety is in line with the results of the absorption and emission spectroscopies (Table 2). The rate constant of epimerization may be correlated to the stability of the enol intermediate. Compounds **1**—**7** showed a linear relationship between ($k+k'$) and triethylamine concentration commonly below 0.2 mol dm^{-3}. The range could depend on the bulkiness of the $C13^4$-substituent, because the rate-determining step is the $C13^2$-deprotonation which can be accelerated by readiness of access of the catalyst to the position of the isomerization or by the size of the catalyst relative to the $C13^4$-substituent. Thus, the epimerization rate constant predominantly depends on the readiness of the molecular transformation accompanied by a change of the $C13^2$-carbon atom from sp^3 to sp^2, rather than the readiness of the $C13^2$-deprotonation. Because the formation of the enol intermediate requires a rearrangement of the $C13^2$-moiety as well as changes in the degree of the ruffling of the macrocycle, it is reasonable that Zn–Chls possessing a bulky $C13^4$-substituent (**6** and **7**) isomerized more slowly than **1**—**5**. Compounds **8** and **9** were distinguished from **1**—**7** by stabilization of the intermediate with electronic effects of the $C13^4$-moieties, which is suggested by a comparison of Chls with variety of macrocycle π-electron densities (Zn–Chl *a*/*a*′, Chl *a*/*a*′, Chl *b*/*b*′, and Pheo *a*/*a*′).[8]

Conclusion

The present study reveals that the deviation between the spectral properties of the paired epimers, the band positions in the absorption and fluorescence emission spectra, the CD intensities, the rate constants and the free energies of epimerization are markers of the ruffling of the chlorin macrocycle. Assuming that Chl *a*′ and BChl *g*′ molecules in vivo are anchored with interactions between the $C13^2$-substituent and the protein matrices of the reaction center complexes, these (*S*)-epimers may suffer from the distortion of the macrocycle, resulting in the change in their photo-redox properties.[23,38] Such a subtle 'tuning', which can more readily occur in the (*S*)-epimers than in the (*R*)-epimers, might be required for the electron or energy-transfer function at particular sites in the reaction center complexes.

Experimental

Materials: HPLC-grade hexane, methanol, 2-propanol, THF, and acetone and reagent-grade diethyl ether and CH_2Cl_2 (Wako) were used as received. Benzene (reagent-grade, Wako) was distilled and stored over molecular sieves 3A. Water purified with a Milli-Q system (Millipore Ltd.) was used throughout.

Pure Chl *a*/*a*′ were prepared as in previous work[12,18] with a slight modification. Briefly, Chls was extracted from lyophilized spinach leaf tissues with CH_2Cl_2, and was demetallated by contact with 10% aqueous hydrochloric acid. The lower black organic phase was washed with an aqueous saturated Na_2CO_3 solution and brine, then dried over Na_2SO_4. After evaporation of the solvent, crude Pheo *a* was purified using a preparative normal-phase HPLC

(column: Senshupak Silica-5251N, 20 mm diameter×250 mm, 4 °C; eluent: hexane/acetone/methanol = 100 : 5 : 1.5).

Preparation of Zn–C13²-demethoxycarbonyl-chlorophyll *a* (= **10**, pyro) was done according to the literature.[39] Reflux of Pheo *a* in 2,4,6-collidine (Wako) followed by isolation using the same HPLC (vide supra) gave C13²-demethoxycarbonyl-pheophytin *a* (pyroPheo *a*). Thus obtained pyroPheo *a* was metallated with Zn(OAc)₂·2H₂O (Wako) in methanol,[25,29] and purified by the abovementioned HPLC system.

Visible absorption spectra of the Chl solutions were recorded on a JASCO spectrophotometer Model V-560. CD and fluorescence measurements were performed on a JASCO spectropolarimeter (Model J-725) and a JASCO fluorescence spectrophotometer (Model FP-777), respectively. Fluorescence emission spectra were corrected using a factor obtained by comparison between a raw spectrum of Chl *a* in methanol and the real one (Oba et al., unpublished result). Proton NMR spectra were recorded on a 270 MHz spectrometer (JEOL GSX-270) in $CDCl_3$ solutions, and ^{13}C NMR spectra were measured in $CDCl_3/CD_3OD$ = 9 : 1 (v/v) solutions on a JEOL JNM-AL400 spectrometer operated at 100.4 MHz (24 °C). MS spectra were obtained using a fast atom bombardment mass spectrometer, JEOL JMS-600H (FAB-matrix, 3-nitrobenzyl alcohol).

Epimerization in Diethyl Ether: The (*R*)-epimer of Zn-Chl (10 μM) was dissolved in diethyl ether containing triethylamine at a concentration from 0.01 to 0.5 mol dm^{-3}. The solution was incubated at 25 °C in the dark, and the temporal change of the C13²-epimeric composition was measured by analytical silica HPLC (column: Senshupak Silica-1251N 4.6 mm diameter×250 mm, 4 °C; eluent: hexane/acetone/methanol = 100 : 5 : 1.5; integrator, Shimadzu C-R6A).

Syntheses of C13⁴-Substituted Pheophytins *a*/*a*′: According to a procedure reported by Shinoda et al.,[27,28] Pheo *a* (30 μmol) was dissolved in dry toluene (10 mL). To this solution was added an equimolar amount of alcohol (R–OH; R = ethyl, isobutyl, neopentyl, decyl, 2-propyl, 2,4-dimethyl-3-pentyl, 2,2,2-trichloroethyl, and benzyl; Wako) and 2 molar amounts of 2-chloro-1-methylpyridinium iodide (Tokyo Kasei) and 4 molar amounts of 4-(dimethylamino)pyridine (Tokyo Kasei). The mixture was refluxed for 3 h under N_2, and then evaporated to dryness. The residue was washed with an aqueous saturated Na_2CO_3 solution and brine, and dried over Na_2SO_4. The title compounds were roughly isolated using flash column chromatography (Wakogel C-200, CH_2Cl_2/diethyl ether = 100 : 2—5), and the preparative HPLC as describe above was used for further purification.

A thus-obtained pheophytin derivative was metallated with Zn(OAc)₂·2H₂O (Wako) in methanol,[25,29] and the product was purified by use of the same HPLC system (for compounds **3**—**5**, and **7**, hexane/acetone/methanol = 100 : 2 : 0.8 was employed as eluent). The integrity of the pigment was confirmed by analytical HPLC. Pigment degradation or epimerization during passage through the silica HPLC column was negligible.[16] All of these products were characterized by ^1H NMR, mass spectrometry, and visible absorption spectra.

C13⁴-Ethyl-pheophytin *a*/*a*′: The retention times were 7.3 (*a*′) and 7.7 min (*a*) by analytical HPLC at a flow rate of 1 mL min^{-1}. Visible (acetone): λ_{max} 665 (relative intensity, 0.43), 607 (0.08), 534 (0.09), 505 (0.10), 410 (1.00). ^1H NMR ($CDCl_3$) δ(C13²-*R*) = 9.40 (s, CH-10), 9.25 (s, CH-5), 8.48 (s, CH-20), 7.88 (dd, *J* = 12, 18 Hz, CH-3¹), 6.19 (dd, *J* = 1, 17 Hz, CH-3²-*cis*), 6.17 (s, CH-13²), 6.08 (dd, *J* = 1, 12 Hz, CH-3²-*trans*), 5.05 (t, *J* = 7 Hz, CH-P²), 4.39 (dq, *J* = 2, 7 Hz, CH-18), 4.22—4.34 (m, CH₂-P¹+CH₂-13⁴), 4.12—4.21 (m, CH-17), 3.60 (s, CH₃-12¹), 3.56 (q, *J* = 8 Hz, CH₂-8¹), 3.31 (s, CH₃-2¹), 3.11 (s, CH₃-7¹), 1.90—2.65 (m, CH₂-17¹,²), 1.80 (t, *J* = 8 Hz, CH₂-P⁴), 1.72 (d, *J* = 7 Hz, CH₃-18), 1.59 (t, *J* = 8 Hz, CH₃-8²), 1.49 (s, CH₃-P¹⁷), 1.20 (t, *J* = 7 Hz, CH₃-13⁵), 0.83—1.62 (m, CH₂-P⁵,⁶,⁸—¹⁰,¹²—¹⁴+CH-P¹⁵,¹⁸,¹⁹), 0.77 (d, *J* = 7 Hz, CH₃-P¹⁶,²⁰), 0.72, 0.70 (2d, *J* = 7 Hz, CH₃-P¹⁸,¹⁹), 0.43, −1.75 (2s, NH). MS (FAB) *m*/*z* (C13²-*R*) 884.4 (MH^+).

^1H NMR ($CDCl_3$) δ(C13²-*S*) = 9.37 (s, CH-10), 9.21 (s, CH-5), 8.41 (s, CH-20), 6.05 (s, CH-13²).

Zinc–C13⁴-ethyl-chlorophyll *a*/*a*′ (= 2, Et): The retention times were 10.0 (*a*′) and 13.5 min (*a*) by analytical HPLC at a flow rate of 1 mL min^{-1}. Visible (acetone): λ_{max} 655 (relative intensity, 0.75), 608 (0.12), 567 (0.07), 425 (1.00), 407 (0.67). ^1H NMR ($CDCl_3$) δ(C13²-*R*) = 9.12 (s, CH-10), 8.88 (s, CH-5), 8.34 (s, CH-20), 7.79 (dd, *J* = 12, 18 Hz, CH-3¹), 6.05 (dd, *J* = 2, 18 Hz, CH-3²-*cis*), 5.96 (dd, *J* = 2, 12 Hz, CH-3²-*trans*), 5.71 (s, CH-13²), 4.91 (t, *J* = 7 Hz, CH-P²), 4.16—4.31 (m, CH-18+CH₂-P¹), 3.93—4.11 (m, CH-17+CH₂-13⁴), 3.39 (s, CH₃-12¹), 3.35 (q, *J* = 7 Hz, CH₂-8¹), 3.24 (s, CH₃-2¹), 2.89 (s, CH₃-7¹), 1.95—2.35 (m, CH₂-17¹,²), 1.77 (t, *J* = 7 Hz, CH₂-P⁴), 1.71 (d, *J* = 7 Hz, CH₃-18), 1.47 (t, *J* = 7 Hz, CH₃-8²), 1.43 (s, CH₃-P¹⁷), 1.19 (t, *J* = 7 Hz, CH₃-13⁵), 0.86—1.55 (m, CH₂-P⁵,⁶,⁸—¹⁰,¹²—¹⁴+CH-P¹⁵,¹⁸,¹⁹), 0.78 (d, *J* = 7 Hz, CH₃-P¹⁶,²⁰), 0.73, 0.71 (2d, *J* = 7 Hz, CH₃-P¹⁸,¹⁹). MS (FAB) *m*/*z* (C13²-*R*) 946.9 (M^+, for ^{64}Zn).

^1H NMR ($CDCl_3$) δ(C13²-*S*) = 9.09 (s, CH-10), 8.85 (s, CH-5), 8.28 (s, CH-20), 6.65 (s, CH-13²).

C13⁴-Isobutyl-pheophytin *a*/*a*′: The retention times were 4.5 (*a*′) and 5.0 min (*a*) by analytical HPLC at a flow rate of 1 mL min^{-1}. Visible (acetone): λ_{max} 665 (relative intensity, 0.43), 608 (0.09), 534 (0.10), 505 (0.11), 410 (1.00). ^1H NMR ($CDCl_3$) δ(C13²-*R*) = 9.52 (s, CH-10), 9.38 (s, CH-5), 8.56 (s, CH-20), 7.98 (dd, *J* = 12, 18 Hz, CH-3¹), 6.28 (dd, *J* = 2, 18 Hz, CH-3²-*cis*), 6.26 (s, CH-13²), 6.17 (dd, *J* = 2, 12 Hz, CH-3²-*trans*), 5.10 (t, *J* = 7 Hz, CH-P²), 4.32—4.53 (m, CH-18+CH₂-P¹), 4.25 (dt, *J* = 1, 8 Hz, CH-17), 4.13, 4.07 (dd, *J* = 7, 11 Hz, CH₂-13⁴), 3.69 (s, CH₃-12¹), 3.67 (q, *J* = 8 Hz, CH₂-8¹), 3.40 (s, CH₃-2¹), 3.22 (s, CH₃-7¹), 2.08—2.70 (m, CH₂-17¹,²), 1.89—1.96 (m, CH-13⁵), 1.86 (t, *J* = 7 Hz, CH₂-P⁴), 1.80 (d, *J* = 7 Hz, CH₃-18), 1.69 (t, *J* = 8 Hz, CH₃-8²), 1.55 (s, CH₃-P¹⁷, 0.90—1.60 (m, CH₂-P⁵,⁶,⁸—¹⁰,¹²—¹⁴+CH-P¹⁵,¹⁸,¹⁹), 0.84, 0.82 (2d, *J* = 7 Hz, CH₃-P¹⁶,²⁰+(CH₃-13⁶)₂), 0.79, 0.77 (2d, *J* = 7 Hz, CH₃-P¹⁸,¹⁹), 0.47, −1.68 (2s, NH). MS (FAB) *m*/*z* (C13²-*R*) 912.4 (MH^+).

^1H NMR ($CDCl_3$) δ(C13²-*S*) = 9.48 (s, CH-10), 9.33 (s, CH-5), 8.49 (s, CH-20), 6.13 (s, CH-13²).

Zinc–C13⁴-isobutyl-chlorophyll *a*/*a*′ (= 3, *i*Bu): The retention times were 8.4 (*a*′) and 9.7 min (*a*) by analytical HPLC at a flow rate of 1 mL min^{-1}. Visible (acetone): λ_{max} 656 (relative intensity, 0.75), 609 (0.14), 566 (0.08), 426 (1.00), 407 (0.70). ^1H NMR ($CDCl_3$) δ(C13²-*R*) = 9.55 (s, CH-10), 9.31 (s, CH-5), 8.45 (s, CH-20), 7.87 (dd, *J* = 11, 18 Hz, CH-3¹), 6.18 (dd, *J* = 2, 18 Hz, CH-3²-*cis*), 6.16 (s, CH-13²), 6.04 (dd, *J* = 2, 11 Hz, CH-3²-*trans*), 5.00 (t, *J* = 7 Hz, CH-P²), 4.18—4.25 (m, CH-18+CH₂-P¹), 4.04—4.25 (m, CH-17+CH₂-13⁴), 3.72 (q, *J* = 8 Hz, CH₂-8¹), 3.66 (s, CH₃-12¹), 3.34 (s, CH₃-2¹), 3.24 (s, CH₃-7¹), 2.22—2.45 (m, CH₂-17¹,²), 1.89—2.18 (m, CH-13⁵), 1.83 (t, *J* = 6 Hz, CH₂-P⁴), 1.80 (d, *J* = 7 Hz, CH₃-18), 1.70 (t, *J* = 8 Hz, CH₃-8²), 1.55 (s, CH₃-P¹⁷), 0.90—1.60 (m, CH₂-P⁵,⁶,⁸—¹⁰,¹²—¹⁴+CH-P¹⁵,¹⁸,¹⁹), 0.87, 0.85 (2d, *J* = 7 Hz, CH₃-P¹⁶,²⁰+(CH₃-13⁶)₂), 0.80, 0.78 (2d, *J* = 7 Hz, CH₃-P¹⁸,¹⁹). MS (FAB) *m*/*z* (C13²-*R*) 975.2 (M^+, for ^{64}Zn).

^1H NMR ($CDCl_3$) δ(C13²-*S*) = 9.52 (s, CH-10), 9.28 (s, CH-5), 8.39 (s, CH-20), 6.09 (s, CH-13²).

C13⁴-Neopentyl-pheophytin *a*/*a*′: The retention times were

4.8 (a') and 4.9 min (a) by analytical HPLC at a flow rate of 1 mL min^{-1}. Visible (acetone): λ_{max} 666 (relative intensity, 0.43), 608 (0.08), 534 (0.10), 505 (0.11), 410 (1.00). ^{1}H NMR ($CDCl_3$) δ(C13^2-*R*) = 9.50 (s, CH-10), 9.34 (s, CH-5), 8.56 (s, CH-20), 7.97 (dd, J = 12, 18 Hz, CH-3^1), 6.27 (s, CH-13^2), 6.25 (dd, J = 1, 18 Hz, CH-3^2-*cis*), 6.15 (dd, J = 1, 12 Hz, CH-3^2-*trans*), 5.10 (t, J = 7 Hz, CH-P^2), 4.32—4.53 (m, CH-18+CH_2-P^1), 4.25—4.37 (m, CH-17), 4.05, 4.01 (d, J = 11 Hz, CH_2-13^4), 3.68 (s, CH_3-12^1), 3.67 (q, J = 8 Hz, CH_2-8^1), 3.39 (s, CH_3-2^1), 3.19 (s, CH_3-7^1), 2.05—2.70 (m, CH_2-17^{1,2}), 1.86 (t, J = 7 Hz, CH_2-P^4), 1.81 (d, J = 7 Hz, CH_3-18), 1.67 (t, J = 8 Hz, CH_3-8^2), 1.55 (s, CH_3-P^{17}), 0.87—1.60 (m, CH_2-P$^{5,6,8—10,12—14}$+CH-P^{15,18,19}), 0.85 (d, J = 7 Hz, CH_3-P^{16,20}), 0.80 (s, $(CH_3$-13$^6)_3$), 0.80, 0.77 (2d, J = 7 Hz, CH_3-P^{18,19}), 0.43, −1.71 (2s, NH). MS (FAB) *m/z* (C13^2-*R*) 926.5 (MH^+).

^{1}H NMR ($CDCl_3$) δ(C13^2-*S*) = 9.46 (s, CH-10), 9.30 (s, CH-5), 8.50 (s, CH-20), 6.14 (s, CH-13^2).

Zinc-C13^4-neopentyl-chlorophyll *a*/*a'* (= 4, *neo*Pn): The retention times were 6.0 (a') and 6.8 min (a) by analytical HPLC at a flow rate of 1 mL min^{-1}. Visible (acetone): λ_{max} 655 (relative intensity, 0.74), 607 (0.13), 564 (0.08), 425 (1.00), 407 (0.67). ^{1}H NMR ($CDCl_3$) δ(C13^2-*R*) = 9.24 (s, CH-10), 8.98 (s, CH-5), 8.43 (s, CH-20), 7.86 (dd, J = 12, 18 Hz, CH-3^1), 6.12 (dd, J = 2, 18 Hz, CH-3^2-*cis*), 6.05 (dd, J = 2, 12 Hz, CH-3^2-*trans*), 5.99 (s, CH-13^2), 4.99 (t, J = 7 Hz, CH-P^2), 4.39 (dq, J = 3, 7 Hz, CH-18), 4.25—4.37 (m, CH_2-P^1+CH-17), 4.03, 3.97 (d, J = 11 Hz, CH_2-13^4), 3.54 (s, CH_3-12^1), 3.45 (q, J = 7 Hz, CH_2-8^1), 3.31 (s, CH_3-2^1), 2.98 (s, CH_3-7^1), 2.00—2.45 (m, CH_2-17^{1,2}), 1.84 (t, J = 7 Hz, CH_2-P^4), 1.82 (d, J = 7 Hz, CH_3-18), 1.55 (t, J = 7 Hz, CH_3-8^2), 1.50 (s, CH_3-P^{17}), 0.88—1.45 (m, CH_2-P$^{5,6,8—10,12—14}$+CH-P^{15,18,19}), 0.85 (d, J = 7 Hz, CH_3-P^{16,20}), 0.84 (s, $(CH_3$-13$^6)_3$), 0.80, 0.78 (2d, J = 7 Hz, CH_3-P^{18,19}). MS (FAB) *m/z* (C13^2-*R*) 989.2 (M^+, for ^{64}Zn).

^{1}H NMR ($CDCl_3$) δ(C13^2-*S*) = 9.21 (s, CH-10), 8.97 (s, CH-5), 8.36 (s, CH-20), 5.90 (s, CH-13^2).

C13^4-Decyl-pheophytin *a*/*a'*: The retention times were 3.9 (a') and 4.0 min (a) by analytical HPLC at a flow rate of 1 mL min^{-1}. Visible (acetone): λ_{max} 666 (relative intensity, 0.45), 608 (0.08), 534 (0.09), 505 (0.11), 410 (1.00). ^{1}H NMR ($CDCl_3$) δ(C13^2-*R*) = 9.50 (s, CH-10), 9.35 (s, CH-5), 8.56 (s, CH-20), 7.97 (dd, J = 12, 18 Hz, CH-3^1), 6.27 (dd, J = 1, 17 Hz, CH-3^2-*cis*), 6.24 (s, CH-13^2), 6.17 (dd, J = 1, 12 Hz, CH-3^2-*trans*), 5.10 (t, J = 7 Hz, CH-P^2), 4.39—4.51 (m, CH-18+CH_2-P^1), 4.20—4.36 (m, CH_2-13^4+CH-17), 3.68 (s, CH_3-12^1), 3.65 (q, J = 8 Hz, CH_2-8^1), 3.39 (s, CH_3-2^1), 3.20 (s, CH_3-7^1), 2.10—2.56 (m, CH_2-17^{1,2}), 1.86 (t, J = 6 Hz, CH_2-P^4), 1.80 (d, J = 7 Hz, CH_3-18), 1.68 (t, J = 8 Hz, CH_3-8^2), 1.55 (s, CH_3-P^{17}), 0.92—1.62 (m, CH_2-13$^{5—12}$+CH_2-P$^{5,6,8—10,12—14}$+CH-P^{15,18,19}), 0.85 (d, J = 7 Hz, CH_3-P^{16,20}), 0.82 (t, J = 7 Hz, CH_3-13^{13}), 0.80, 0.77 (2d, J = 7 Hz, CH_3-P^{18,19}), 0.44, −1.69 (2s, NH). MS (FAB) *m/z* (C13^2-*R*) 996.5 (MH^+).

^{1}H NMR ($CDCl_3$) δ(C13^2-*S*) = 9.46 (s, CH-10), 9.31 (s, CH-5), 8.50 (s, CH-20), 6.10 (s, CH-13^2).

Zinc-C13^4-decyl-chlorophyll *a*/*a'* (= 5, C_{10}): The retention times were 5.2 (a') and 6.1 min (a) by analytical HPLC at a flow rate of 1.0 mL min^{-1}. Visible (acetone): λ_{max} 655 (relative intensity, 0.74), 608 (0.14), 565 (0.09), 425 (1.00), 407 (0.70). ^{1}H NMR ($CDCl_3$) δ(C13^2-*R*) = 9.32 (s, CH-10), 9.07 (s, CH-5), 8.43 (s, CH-20), 7.90 (dd, J = 12, 18 Hz, CH-3^1), 6.15 (dd, J = 1, 18 Hz, CH-3^2-*cis*), 6.05 (dd, J = 1, 12 Hz, CH-3^2-*trans*), 5.88 (s, CH-13^2), 4.97 (t, J = 7 Hz, CH-P^2), 4.37 (1H, dq, J = 2, 7 Hz, CH-18), 4.24 (2H, dt, J = 2, 7 Hz, CH_2-P^1), 4.02—4.18 (m, CH_2-13^4+CH-17), 3.52 (s, CH_3-12^1), 3.50 (q, J = 7 Hz, CH_2-8^1), 3.33 (s, CH_3-2^1), 3.06 (s, CH_3-7^1), 2.20—2.41, 2.03—2.16 (m, CH_2-17^{1,2}), 1.83 (t, J = 8 Hz, CH_2-P^4), 1.79 (d, J = 7 Hz, CH_3-18), 1.59 (t, J = 7 Hz, CH_3-8^2), 1.49 (s, CH_3-P^{17}), 0.88—1.68 (m, CH_2-13$^{5—12}$+CH_2-P$^{5,6,8—10,12—14}$+CH-P^{15,18,19}), 0.85 (d, J = 7 Hz, CH_3-P^{16,20}), 0.82 (t, J = 7 Hz, CH_3-13^{13}), 0.80, 0.77 (2d, J = 7 Hz, CH_3-P^{18,19}). MS (FAB) *m/z* (C13^2-*R*) 1059.0 (M^+, for ^{64}Zn).

^{1}H NMR ($CDCl_3$) δ(C13^2-*S*) = 9.29 (s, CH-10), 9.04 (s, CH-5), 8.37 (s, CH-20), 5.81 (s, CH-13^2).

C13^4-Isopropyl-pheophytin *a*/*a'*: The retention times were 5.8 (a') and 6.0 min (a) by analytical HPLC at a flow rate of 1 mL min^{-1}. Visible (acetone): λ_{max} 665 (relative intensity, 0.42), 608 (0.09), 534 (0.10), 505 (0.11), 410 (1.00). ^{1}H NMR ($CDCl_3$) δ(C13^2-*R*) = 9.50 (s, CH-10), 9.35 (s, CH-5), 8.57 (s, CH-20), 7.97 (dd, J = 12, 18 Hz, CH-3^1), 6.27 (dd, J = 2, 18 Hz, CH-3^2-*cis*), 6.21 (s, CH-13^2), 6.16 (dd, J = 2, 12 Hz, CH-3^2-*trans*), 5.23—5.37 (m, CH-13^4), 5.12 (t, J = 7 Hz, CH-P^2), 4.37—4.52 (m, CH-18+CH_2-P^1), 4.26 (dt, J = 2, 8 Hz, CH-17), 3.68 (s, CH_3-12^1), 3.64 (q, J = 8 Hz, CH_2-8^1), 3.39 (s, CH_3-2^1), 3.20 (s, CH_3-7^1), 2.05—2.68 (m, CH_2-17^{1,2}), 1.87 (t, J = 8 Hz, CH_2-P^4), 1.80 (d, J = 7 Hz, CH_3-18), 1.67 (t, J = 8 Hz, CH_3-8^2), 1.56 (s, CH_3-P^{17}), 1.29, 1.25 (2d, J = 6 Hz, $(CH_3$-13$^5)_2$), 0.83—1.65 (m, CH_2-P$^{5,6,8—10,12—14}$+CH-P^{15,18,19}), 0.84 (d, J = 7 Hz, CH_3-P^{16,20}), 0.80, 0.77 (2d, J = 7 Hz, CH_3-P^{18,19}), 0.44, −1.71 (2s, NH). MS (FAB) *m/z* (C13^2-*R*) 989.5 (MH^+).

^{1}H NMR ($CDCl_3$) δ(C13^2-*S*) = 9.46 (s, CH-10), 9.30 (s, CH-5), 8.50 (s, CH-20), 6.08 (s, CH-13^2).

Zinc-C13^4-isopropyl-chlorophyll *a*/*a'* (= 6, *i*Pr): The retention times were 6.8 (a') and 8.9 min (a) by analytical HPLC at a flow rate of 1 mL min^{-1}. Visible (acetone): λ_{max} 655 (relative intensity, 0.74), 608 (0.13), 565 (0.07), 426 (1.00), 407 (0.66). ^{1}H NMR ($CDCl_3$) δ(C13^2-*R*) = 9.34 (s, CH-10), 9.10 (s, CH-5), 8.45 (s, CH-20), 7.92 (dd, J = 12, 18 Hz, CH-3^1), 6.15 (dd, J = 1, 18 Hz, CH-3^2-*cis*), 6.05 (dd, J = 1, 12 Hz, CH-3^2-*trans*), 5.92 (s, CH-13^2), 5.23—5.33 (m, CH-13^4), 5.00 (t, J = 7 Hz, CH-P^2), 4.40 (dq, J = 2, 7 Hz, CH-18), 4.10—4.25 (m, CH_2-P^1+CH-17), 3.55 (s, CH_3-12^1), 3.53 (q, J = 8 Hz, CH_2-8^1), 3.33 (s, CH_3-2^1), 3.06 (s, CH_3-7^1), 2.07—2.50 (m, CH_2-17^{1,2}), 1.83 (t, J = 8 Hz, CH_2-P^4), 1.79 (d, J = 7 Hz, CH_3-18), 1.59 (t, J = 8 Hz, CH_3-8^2), 1.51 (s, CH_3-P^{17}), 1.31, 1.25 (2d, J = 6 Hz, $(CH_3$-13$^5)_2$), 0.88—1.65 (m, CH_2-P$^{5,6,8—10,12—14}$+CH-P^{15,18,19}), 0.85 (d, J = 7 Hz, CH_3-P^{16,20}), 0.82, 0.78 (2d, J = 7 Hz, CH_3-P^{18,19}). MS (FAB) *m/z* (C13^2-*R*) 961.2 (M^+, for ^{64}Zn).

^{1}H NMR ($CDCl_3$) δ(C13^2-*S*) = 9.31 (s, CH-10), 9.07 (s, CH-5), 8.37 (s, CH-20), 5.81 (s, CH-13^2).

C13^4-2,4-Dimethyl-3-pentyl-pheophytin *a*/*a'*: The retention times were 4.4 (a') and 4.5 min (a) by analytical HPLC at a flow rate of 1 mL min^{-1}. Visible (acetone): λ_{max} 666 (relative intensity, 0.45), 608 (0.07), 534 (0.08), 505 (0.10), 410 (1.00). ^{1}H NMR ($CDCl_3$) δ(C13^2-*R*) = 9.51 (s, CH-10), 9.35 (s, CH-5), 8.57 (s, CH-20), 7.99 (dd, J = 12, 18 Hz, CH-3^1), 6.26 (s, CH-13^2), 6.25 (dd, J = 1, 18 Hz, CH-3^2-*cis*), 6.15 (dd, J = 1, 12 Hz, CH-3^2-*trans*), 5.07 (t, J = 7 Hz, CH-P^2), 4.79 (t, J = 6 Hz, CH-13^4), 4.30—4.60 (m, CH-18+CH_2-P^1+CH-17), 3.69 (s, CH_3-12^1), 3.64 (q, J = 8 Hz, CH_2-8^1), 3.39 (s, CH_3-2^1), 3.19 (s, CH_3-7^1), 2.04—2.75 (m, CH_2-17^{1,2}), 1.84 (t, J = 8 Hz, CH_2-P^4), 1.80 (d, J = 7 Hz, CH_3-18), 1.67 (t, J = 8 Hz, CH_3-8^2), 1.54 (s, CH_3-P^{17}), 1.04, 0.92, 0.64, 0.43 (4d, J = 6 Hz, $(CH_3$-13$^6)_4$), 0.88—1.64 (m, $(CH$-13$^5)_2$+CH_2-P$^{5,6,8—10,12—14}$+CH-P^{15,18,19}), 0.84 (d, J = 7 Hz, CH_3-P^{16,20}), 0.79, 0.76 (2d, J = 7 Hz, CH_3-P^{18,19}), 0.35, −1.75 (2s, NH). MS (FAB) *m/z* (C13^2-*R*) 954.3 (MH^+).

^{1}H NMR ($CDCl_3$) δ(C13^2-*S*) = 9.45 (s, CH-10), 9.28 (s, CH-5), 8.45 (s, CH-20), 6.07 (s, CH-13^2).

Zinc-C13^4-2,4-dimethyl-3-pentyl-chlorophyll *a*/*a'* (= 7, CH*i*Pr$_2$): The retention times were 4.9 (a') and 6.0 min (a) by analytical HPLC at a flow rate of 1 mL min^{-1}. Visible (ace-

tone): λ_{max} 656 (relative intensity, 0.70), 608 (0.12), 566 (0.06), 426 (1.00), 407 (0.65). ^{1}H NMR ($CDCl_3$) δ(C13^2-*R*) = 9.38 (s, CH-10), 9.14 (s, CH-5), 8.45 (s, CH-20), 7.92 (dd, *J* = 12, 18 Hz, CH-3^1), 6.15 (dd, *J* = 2, 18 Hz, CH-3^2-*cis*), 6.05 (dd, *J* = 2, 12 Hz, CH-3^2-*trans*), 6.13 (s, CH-13^2), 4.92 (t, *J* = 7 Hz, CH-P^2), 4.68 (1H, t, *J* = 6 Hz, CH-13^4), 4.33 (dq, *J* = 2, 7 Hz, CH-18), 4.15—4.23 (m, CH-17), 3.93—4.06 (m, CH_2-P^1), 3.55 (q, *J* = 7 Hz, CH_2-8^1), 3.47 (s, CH_3-12^1), 3.34 (s, CH_3-2^1), 3.08 (s, CH_3-7^1), 1.95—2.35 (m, CH_2-17^{1,2}), 1.87 (t, *J* = 7 Hz, CH_2-P^4), 1.73 (d, *J* = 7 Hz, CH_3-18), 1.62 (t, *J* = 7 Hz, CH_3-8^2), 1.47 (s, CH_3-P^{17}), 0.95, 0.85, 0.59, 0.39 (4d, *J* = 6 Hz, (CH_3-13^6)$_4$), 0.89—1.55 (m, (CH-13^5)$_2$+CH_2-P$^{5,6,8—10,12—14}$+CH-P^{15,18,19}), 0.85 (d, *J* = 7 Hz, CH_3-P^{16,20}), 0.81, 0.78 (2d, *J* = 7 Hz, CH_3-P^{18,19}). MS (FAB) *m/z* (C13^2-*R*) 1017.1 (M^+, for ^{64}Zn).

^{1}H NMR ($CDCl_3$) δ(C13^2-*S*) = 9.31 (s, CH-10), 9.07 (s, CH-5), 8.32 (s, CH-20), 6.01 (s, CH-13^2).

C13^4-2,2,2-Trichloroethyl-pheophytin *a*/*a*′: The retention times were 5.2 (*a*′) and 5.4 min (*a*) by analytical HPLC at a flow rate of 1 mL min^{-1}. Visible (acetone): λ_{max} 665 (relative intensity, 0.42), 607 (0.09), 534 (0.10), 505 (0.11), 410 (1.00). ^{1}H NMR ($CDCl_3$) δ(C13^2-*R*) = 9.50 (s, CH-10), 9.35 (s, CH-5), 8.55 (s, CH-20), 7.97 (dd, *J* = 11, 18 Hz, CH-3^1), 6.40 (s, CH-13^2), 6.28 (dd, *J* = 1, 18 Hz, CH-3^2-*cis*), 6.18 (dd, *J* = 1, 12 Hz, CH-3^2-*trans*), 5.07 (t, *J* = 7 Hz, CH-P^2), 5.05, 5.00 (d, *J* = 12 Hz, CH_2-13^4), 4.30—4.60 (m, CH-18+CH_2-P^1+CH-17), 3.68 (s, CH_3-12^1), 3.66 (q, *J* = 8 Hz, CH_2-8^1), 3.39 (s, CH_3-2^1), 3.21 (s, CH_3-7^1), 2.05—2.70 (m, CH_2-17^{1,2}), 1.86 (t, *J* = 7 Hz, CH_2-P^4), 1.81 (d, *J* = 7 Hz, CH_3-18), 1.68 (t, *J* = 8 Hz, CH_3-8^2), 1.56 (s, CH_3-P^{17}), 0.87—1.65 (m, CH_2-P$^{5,6,8—10,12—14}$+CH-P^{15,18,19}), 0.85 (d, *J* = 7 Hz, CH_3-P^{16,20}), 0.80, 0.78 (2d, *J* = 7 Hz, CH_3-P^{18,19}) 0.35, −1.75 (2s, NH). MS (FAB) *m/z* (C13^2-*R*) 987.4 (MH^+).

^{1}H NMR ($CDCl_3$) δ(C13^2-*S*) = 9.48 (s, CH-10), 9.32 (s, CH-5), 8.49 (s, CH-20), 6.26 (s, CH-13^2).

Zinc- C13^4- 2, 2, 2- trichloroethyl- chlorophyll *a*/*a*′ (= 8, CH_2CCl_3): The retention times were 7.5 (*a*′) and 9.0 min (*a*) by analytical HPLC at a flow rate of 1 mL min^{-1}. Visible (acetone): λ_{max} 656 (relative intensity, 0.71), 608 (0.13), 566 (0.07), 426 (1.00), 407 (0.70). ^{1}H NMR ($CDCl_3$) δ(C13^2-*R*) = 9.38 (s, CH-10), 9.14 (s, CH-5), 8.44 (s, CH-20), 7.92 (dd, *J* = 12, 18 Hz, CH-3^1), 6.16 (dd, *J* = 2, 18 Hz, CH-3^2-*cis*), 6.12 (s, CH-13^2), 6.06 (dd, *J* = 2, 12 Hz, CH-3^2-*trans*), 4.92—5.06 (m, CH-P^2+CH_2-13^4), 4.40 (dq, *J* = 2, 7 Hz, CH-18), 4.27 (dt, *J* = 2, 7 Hz, CH-17), 4.17 (t, *J* = 7 Hz, CH_2-P^1), 3.57 (q, *J* = 8 Hz, CH_2-8^1), 3.56 (s, CH_3-12^1), 3.33 (s, CH_3-2^1), 3.10 (s, CH_3-7^1), 1.95—2.50 (m, CH_2-17^{1,2}), 1.80 (d, *J* = 7 Hz, CH_3-18), 1.75—1.88 (m, CH_2-P^4), 1.61 (t, *J* = 8 Hz, CH_3-8^2), 1.50 (s, CH_3-P^{17}), 0.88—1.76 (m, CH_2-P$^{5,6,8—10,12—14}$+CH-P^{15,18,19}), 0.85 (d, *J* = 7 Hz, CH_3-P^{16,20}), 0.81, 0.78 (2d, *J* = 7 Hz, CH_3-P^{18,19}). MS (FAB) *m/z* (C13^2-*R*) 1050.1 (M^+, for ^{64}Zn).

^{1}H NMR ($CDCl_3$) δ(C13^2-*S*) = 9.35 (s, CH-10), 9.11 (s, CH-5), 8.38 (s, CH-20), 6.01 (s, CH-13^2).

C13^4-Benzyl-pheophytin *a*/*a*′: The retention times were 5.1 (*a*′) and 6.1 min (*a*) by analytical HPLC at a flow rate of 1 mL min^{-1}. Visible (acetone): λ_{max} 666 (relative intensity, 0.44), 608 (0.08), 534 (0.09), 505 (0.11), 410 (1.00). ^{1}H NMR ($CDCl_3$) δ(C13^2-*R*) = 9.48 (s, CH-10), 9.33 (s, CH-5), 8.51 (s, CH-20), 7.96 (dd, *J* = 11, 18 Hz, CH-3^1), 7.36—7.26 (m, CH-phenyl), 6.31 (s, CH-13^2), 6.26 (dd, *J* = 2, 18 Hz, CH-3^2-*cis*), 6.16 (dd, *J* = 2, 11 Hz, CH-3^2-*trans*), 5.43, 5.34 (d, *J* = 12 Hz, CH_2-13^4), 5.12 (t, *J* = 7 Hz, CH-P^2), 4.23—4.58 (m, CH-18+CH_2-P^1), 3.93—4.02 (m, CH-17), 3.69 (s, CH_3-12^1), 3.65 (q, *J* = 7 Hz, CH_2-8^1), 3.38 (s, CH_3-2^1), 3.19 (s, CH_3-7^1), 2.03—2.62 (m, CH_2-17^{1,2}), 1.88 (t, *J* = 6 Hz, CH_2-P^4), 1.68 (d, *J* = 7 Hz, CH_3-18), 1.59 (t, *J* = 7 Hz, CH_3-8^2), 1.57 (s, CH_3-P^{17}), 0.92—1.55 (m, CH_2-P$^{5,6,8—10,12—14}$+CH-P^{15,18,19}), 0.85 (d, *J* = 7 Hz, CH_3-P^{16,20}), 0.80, 0.78 (2d, *J* = 7 Hz, CH_3-P^{18,19}), 0.48, −1.68 (2s, NH). MS (FAB) *m/z* (C13^2-*R*) 946.3 (MH^+).

^{1}H NMR ($CDCl_3$) δ(C13^2-*S*) = 9.45 (s, CH-10), 9.29 (s, CH-5), 8.49 (s, CH-20), 6.20 (s, CH-13^2).

Zinc-C13^4-benzyl-chlorophyll *a*/*a*′ (= 9, Bzl): The retention times were 10.6 (*a*′) and 13.5 min (*a*) by analytical HPLC at a flow rate of 1.0 mL min^{-1}. Visible (acetone): λ_{max} 656 (relative intensity, 0.77), 608 (0.13), 566 (0.07), 426 (1.00), 407 (0.68). ^{1}H NMR ($CDCl_3$) δ(C13^2-*R*) = 9.32 (s, CH-10), 9.07 (s, CH-5), 8.37 (s, CH-20), 7.89 (dd, *J* = 11, 18 Hz, CH-3^1), 7.25—7.37 (m, CH-phenyl), 6.13 (dd, *J* = 2, 18 Hz, CH-3^2-*cis*), 6.04 (dd, *J* = 2, 11 Hz, CH-3^2-*trans*), 5.97 (s, CH-13^2), 5.35, 5.26 (d, *J* = 12 Hz, CH_2-13^4), 4.99 (t, *J* = 4 Hz, CH-P^2), 4.04—4.28 (m, CH-18+CH_2-P^1), 3.77—3.87 (m, CH-17), 3.54 (q, *J* = 8 Hz, CH_2-8^1), 3.53 (s, CH_3-12^1), 3.31 (s, CH_3-2^1), 3.06 (s, CH_3-7^1), 1.97—2.34 (m, CH_2-17^{1,2}), 1.83 (t, *J* = 8 Hz, CH_2-P^4), 1.64 (d, *J* = 7 Hz, CH_3-18), 1.59 (t, *J* = 8 Hz, CH_3-8^2), 1.49 (s, CH_3-P^{17}), 0.90—1.60 (m, CH_2-P$^{5,6,8—10,12—14}$+CH-P^{15,18,19}), 0.85 (d, *J* = 7 Hz, CH_3-P^{16,20}), 0.80, 0.78 (2d, *J* = 7 Hz, CH_3-P^{18,19}). MS (FAB) *m/z* (C13^2-*R*) 1009.1 (M^+, for ^{64}Zn).

^{1}H NMR ($CDCl_3$) δ(C13^2-S) = 9.29 (s, CH-10), 9.04 (s, CH-5), 8.32 (s, CH-20), 5.90 (s, CH-13^2).

Molecular Modeling Calculation of Zn–Chls: Molecular modelings were performed using a program package HyperChem version 5.1 (HyperCube, Inc.) on a computer Dell Dimension XPS T-500. Molecular mechanics program MM+ and quantum mechanics program PM3 were employed without any modification of the provided parameters (stop criterion, energy gradient < 0.01 kcal Å^{-1} mol^{-1}). In these models, the C17-phytyl chain was replaced with a methyl group, and the solvent effect was neglected. The molecular structure was initially optimized by MM+, and then the obtained structure was optimized again by PM3. Alternate calculations with MM+/PM3 were continued until the energy of the model structure became almost unchanged.[24]

The authors are grateful to Mr. S. Kawaguchi (Univ. of Tokyo) for molecular modeling calculations, Messrs. A. Nakamura and M. Kawamura (Univ. of Tokyo) for helpful advice.

References

1 F. W. Bobe, N. Pfennig, K. L. Swanson, and K. M. Smith, *Biochemistry*, **29**, 4340 (1990).

2 J. Chiefari, K. Griebenow, N. Griebenow, T. S. Balaban, A. R. Holzwarth, and K. Schaffner, *J. Phys. Chem.*, **99**, 1357 (1995).

3 H. Tamiaki, *Coord. Chem. Rev.*, **148**, 183 (1996).

4 A. Nakamura and T. Watanabe, *FEBS Lett.*, **426**, 201 (1998).

5 H. Maeda, T. Watanabe, M. Kobayashi, and I. Ikegami, *Biochim. Biophys. Acta*, **1099**, 74 (1992).

6 M. Kobayashi, E. J. van de Meent, C. Erkelens, J. Amesz, I. Ikegami, and T. Watanabe, *Biochim. Biophys. Acta*, **1057**, 89 (1991).

7 M. Kobayashi, T. Watanabe, I. Ikegami, E. J. van de Meent, and J. Amesz, *FEBS Lett.*, **284**, 129 (1991).

8 H. Mazaki, T. Watanabe, T. Takahashi, A. Struck, and H. Scheer, *Bull. Chem. Soc. Jpn.*, **65**, 3080 (1992).

9 S. Lötjönen and P. H. Hynninen, *Org. Magn. Reson.*, **16**, 304 (1981).

10 S. Lötjönen and P. H. Hynninen, *Org. Magn. Reson.*, **21**, 757 (1983).

11 P. H. Hynninen and G. Sievers, *Z. Naturforsh., B*, **36b**, 1000 (1981).
12 T. Watanabe, A. Hongu, K. Honda, M. Nakazato, M. Konno, and S. Saitoh, *Anal. Chem.*, **56**, 251 (1984).
13 P. H. Hynninen, M. R. Wasielewski, and J. J. Katz, *Acta Chem. Scand.*, **B33**, 637 (1979).
14 P. H. Hynninen, *J. Chromatogr.*, **175**, 89 (1979).
15 H. Mazaki and T. Watanabe, *Bull. Chem. Soc. Jpn.*, **61**, 2969 (1988).
16 T. Oba, M. Kobayashi, S. Yoshida, and T. Watanabe, *Anal. Sci.*, **12**, 281 (1996).
17 T. Watanabe, M. Kobayashi, A. Hongu, and T. Oba, *Chem. Lett.*, **1992**, 1847.
18 T. Oba, T. Watanabe, M. Mimuro, M. Kobayashi, and S. Yoshida, *Photochem. Photobiol.*, **63**, 639 (1996).
19 T. Oba, M. Mimuro, Z.-Y. Wang, T. Nozawa, S. Yoshida, and T. Watanabe, *J. Phys. Chem. B*, **101**, 3261 (1997).
20 T. Oba, H. Furukawa, Z.-Y. Wang, T. Nozawa, M. Mimuro, H. Tamiaki, and T. Watanabe, *J. Phys. Chem. B*, **102**, 7882 (1998).
21 H. Furukawa, T. Oba, H. Tamiaki, and T. Watanabe, *J. Phys. Chem. B*, **103**, 7398 (1999).
22 L. K. Hanson, "Chlorophylls," ed by H. Scheer, CRC Press, Boca Raton (1991), Chap. 4.9.
23 E. Gudowska-Nowak, M. D. Newton, and J. Fajer, *J. Phys. Chem.*, **94**, 5795 (1990).
24 Y. Kureishi and H. Tamiaki, *J. Porphyrins Phthalocyanines*, **2**, 159 (1998).
25 H. Tamiaki, S. Takeuchi, S. Tsudzuki, T. Miyatake, and R. Tanikaga, *Tetrahedron*, **54**, 6699 (1998).
26 P. H. Hynninen and S. Lötjönen, *Magn. Reson. Chem.*, **23**, 605 (1985).
27 S. Shinoda and A. Osuka, *Tetrahedron Lett.*, **37**, 4945 (1996).
28 S. Shinoda, H. Tsukube, Y. Nishimura, I. Yamazaki, and A. Osuka, *Tetrahedron*, **53**, 13657 (1997).
29 T. Oba and H. Tamiaki, *Photosynth. Res.*, **61**, 23 (1999).
30 F. C. Pennington, H. H. Strain, W. A. Svec, and J. J. Katz, *J. Am. Chem. Soc.*, **86**, 1418 (1964).
31 C. Houssier and K. Sauer, *J. Am. Chem. Soc.*, **92**, 779 (1970).
32 T. Watanabe, H. Mazaki, and M. Nakazato, *Biochim. Biophys. Acta*, **892**, 197 (1987).
33 The resonance peaks at the C18-positions of the (*S*)-epimers could not be identified, probably owing to its accidental coincidence with one of the solvent signals.
34 N. Risch and H. Brockman, Jr., *Tetrahedron Lett.*, **24**, 173 (1983).
35 H.-C. Chow, R. Serlin, and C. E. Strouse, *J. Am. Chem. Soc.*, **97**, 7230 (1975).
36 H. Wolf and H. Scheer, *Ann. N. Y. Acad. Sci.*, **206**, 549 (1973).
37 S. Krawczyk, *Biochim. Biophys. Acta*, **976**, 140 (1989).
38 K. M. Barkigia, L. Chantranupong, K. M. Smith, and J. Fajer, *J. Am. Chem. Soc.*, **110**, 7566 (1988).
39 K. M. Smith, D. A. Goff, and D. J. Simpson, *J. Am. Chem. Soc.*, **107**, 4946 (1985).